Molecular Structure and Vibrational Spectroscopic Investigation of Secnidazole Using Density Functional Theory

Soni Mishra, Deepika Chaturvedi, Poonam Tandon,* and V. P. Gupta

Department of Physics, University of Lucknow, Lucknow 226007, India

A. P. Ayala and S. B. Honorato

Departamento de Física, Universidade Federal do Ceará, C. P. 6030, 60.455-900 Fortaleza, CE, Brazil

H. W. Siesler

Department of Physical Chemistry, University of Duisburg-Essen, Essen D45117, Germany

Received: June 19, 2008; Revised Manuscript Received: October 7, 2008

Secnidazole (α,2-dimethyl-5-nitro-1*H*-imidazole-1-ethanol) is an antimicrobical drug, and it is particularly effective in the treatment of amebiasis, giardiasis, trichomoniasis, and bacterial vaginosis. Secnidazole crystallizes as a hemihydrate, which belongs to a monoclinic system having space group $P2_1/c$, with a = 12.424 Å, b = 12.187 Å, c = 6.662 Å, and β = 100.9°. The optimized geometries and total energies of different conformers of the secnidazole molecule have been determined by the method of density functional theory (DFT). For both geometry and total energy, it has been combined with B3LYP functionals having extended basis sets 4-31G, 6-31G, and 6-311++G(d,p) for each of the three stable conformers of secnidazole. Using this optimized structure, we have calculated the infrared and Raman wavenumbers and compared them with the experimental data. The calculated wavenumbers are in an excellent agreement with the experimental values. Based on these results, we have discussed the correlation between the vibrational modes and the crystalline structure of the most stable conformer of secnidazole. A complete assignment is provided for the observed Raman and IR spectra.

I. Introduction

Secnidazole (α,2-dimethyl-5-nitro-1*H*-imidazole-1-ethanol; Figure 1) is used as an antiprotozoal, antiamebic, and antibacterial drug.[1] It is an antimicrobic agent which is structurally related to the commonly used 5-nitromidazoles metronidazole and tinidazole. Secnidazole is particularly effective in the treatment of amebiasis, giardiasis, trichomoniasis, and bacterial vaginosis[2] as it is rapidly and completely absorbed after oral administration and has a longer terminal elimination half-life (17−29 h) than commonly used drugs in this class.[3] In these cases, the treatment with secnidazole is shorter and significantly more effective than the treatment using other imidazole drugs and the adverse effects are not very drastic.[4]

As an anhydrous solid, secnidazole is not stable at standard conditions. Single crystal structure determinations showed that this compound crystallizes in a hemihydrate form having four secnidazole molecules per unit cell (Z = 4) and two water molecules. Secnidazole hemihydrate belongs to a monoclinic system, space group $P2_1/c$, with a = 12.424 Å, b = 12.187 Å, c = 6.662 Å, and β = 100.9°.[5] The water molecules present in the structure are shared among four half-occupied sites and are linked to a propyl radical forming hydrogen bonds of the form head−tail. The molecules are held together forming dimers by means of a hydrogen bond between the OH group and a water molecule.[5] The structure of secnidazole is of some interest as it possesses a strong electron attracting nitro group as well as a strong electron donating OH group and has the possibilities of intramolecular as well as intermolecular hydrogen bonding.

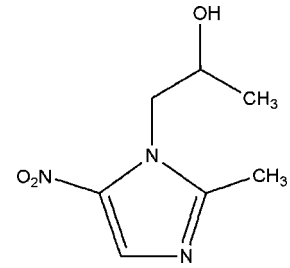

Figure 1. Schematic of the secnidazole molecule.

Internal rotation about a C−C bond may result in several isomeric conformations.

In the present work, the conformational stability of the secnidazole molecule was investigated through quantum mechanical calculations. Geometry optimizations of the possible stable rotamers were performed, and the corresponding relative energies were compared. A complete vibrational analysis of secnidazole was performed by combining Raman and infrared data with quantum mechanical calculations. Infrared and Raman spectroscopies are among the traditional methods of analysis, and particularly powerful for nondestructive characterization of substances including living material.[6] The calculated vibrational spectra were analyzed on the basis of the potential energy distribution (PED) of each vibrational mode, which allowed us to obtain a quantitative as well as qualitative interpretation of the infrared and Raman spectra.

* Author for correspondence. E-mail: poonam_tandon@hotmail.com.

10.1021/jp805399h CCC: $40.75
Published on Web 12/15/2008

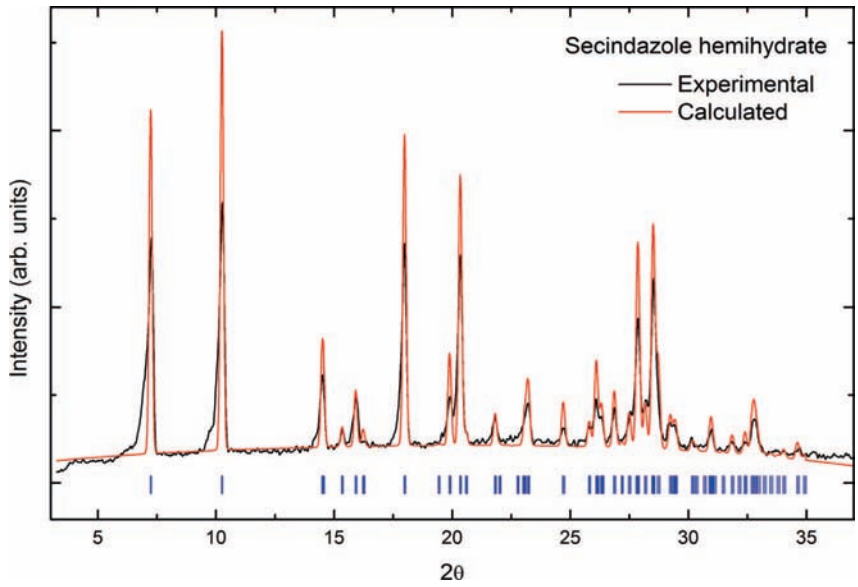

Figure 2. Comparison of the experimental and calculated (from secnidazole hemihydrate crystalline structure) X-ray powder pattern.

II. Experimental Details

Secnidazole samples were characterized by X-ray powder diffraction in order to identify the corresponding solid form. The experimental and simulated powder diffraction patterns of secnidazole are shown in Figure 2. The FULLPROF program[7] was used to fit the simulated pattern to the experimental one, and some instrumental parameters (overall intensity, background, zero shift, etc.) were also adjusted. An excellent agreement between the simulated powder pattern based on the reported crystalline structure and the experimental data clearly show that our samples are in the hemihydrate form.

Infrared spectra were recorded on a Bruker IFS28 FT-IR spectrometer with a spectral resolution of 4 cm^{-1}. KBr pellets of solid samples were prepared from mixtures of 200 mg KBr with 1 mg of sample using a hydraulic press. Raman spectra were measured using a Jobin Yvon T6400 subtractive triple spectrometer equipped with a liquid nitrogen cooled CCD detector, and the 514.5 nm radiation from an Ar^+ laser was used as the excitation line.

III. Computational Details

The electronic structure and optimized geometries of the stable conformers of the molecule were computed by the DFT method[8] using the Gaussian 03 program[9] package employing 6-311++G(d,p) basis sets and Becke's three parameter (local, nonlocal, Hartree−Fock) hybrid exchange functionals with Lee−Yang−Parr correlation functionals (B3LYP).[10−12] The basis set 6-311++G(d,p) augmented by d polarization functions on heavy atoms and p polarization functions on hydrogen atoms as well as diffuse functions for both hydrogen and heavy atoms were used.[13,14] The absolute Raman intensities and infrared absorption intensities were calculated in the harmonic approximation, at the same level of theory as used for the optimized geometries, from the derivatives of the dipole moment and polarizability of each normal mode, respectively. The normal-mode analysis was performed, and the PED was calculated for each of the internal coordinates using localized symmetry.[15,16] For this purpose a complete set of 66 internal coordinates was defined using Pulay's recommendations.[15,16] The vibrational assignments of the normal modes were proposed on the basis of the PED calculated using the program GAR2PED.[17] Raman and infrared spectra were simulated using a pure Lorentzian band profile (fwhm = 8 cm^{-1}) using indigenously developed software. Visualization and confirmation of the calculated forms of the vibrations were done using the CHEMCRAFT program.[18]

IV. Results and Discussion

A. Geometry Optimization and Energies. Geometry optimization calculations were started taking the secnidazole conformation determined by single crystal X-ray diffraction[5] as the initial geometry. The geometry optimization produced a molecule which is remarkably similar to one of the crystallographic asymmetric unit. The optimized and experimental structures of the molecule were compared by superimposing them using a least-squares algorithm that minimizes the distances between the corresponding non-hydrogen atoms (Figure 3a). The agreement between the optimized geometry and the experimental crystal structure is excellent showing that the geometry optimization almost exactly reproduces the experimental conformation (overall average deviation 0.078 Å). The main differences lie in the misorientation of the methyl and hydroxyl groups. The latter one exhibits the largest deviation from the experimental results, but this effect may be associated with the O13H···Ow and O13H···N4 hydrogen bonds, which stabilize the crystalline structure.

There is a chiral carbon in the molecular geometry of secnidazole, but racemic secnidazole is used in clinical trials at the present time. Three different configurations have been obtained based on the orientations of the ethanol moiety. The equilibrium geometry of each conformer has been determined by the energy minimization. These calculations were carried out with the basis sets 4-31G, 6-31G, and 6-311++G(d,p). The relative energies of these three conformers for which optimized geometries were found are given in Table 1. The different conformers are shown in Figure 3b. Conformer **I** is more stable than conformers **II** and **III**. The energy difference between conformer **I** and conformer **II** is 0.8838 kcal mol^{-1}, and that between conformer **I** and conformer **III** is 2.6738 kcal mol^{-1} for the basis set 6-311++G(d,p). Since these energy differences are much larger than kT (at room temperature), there is almost

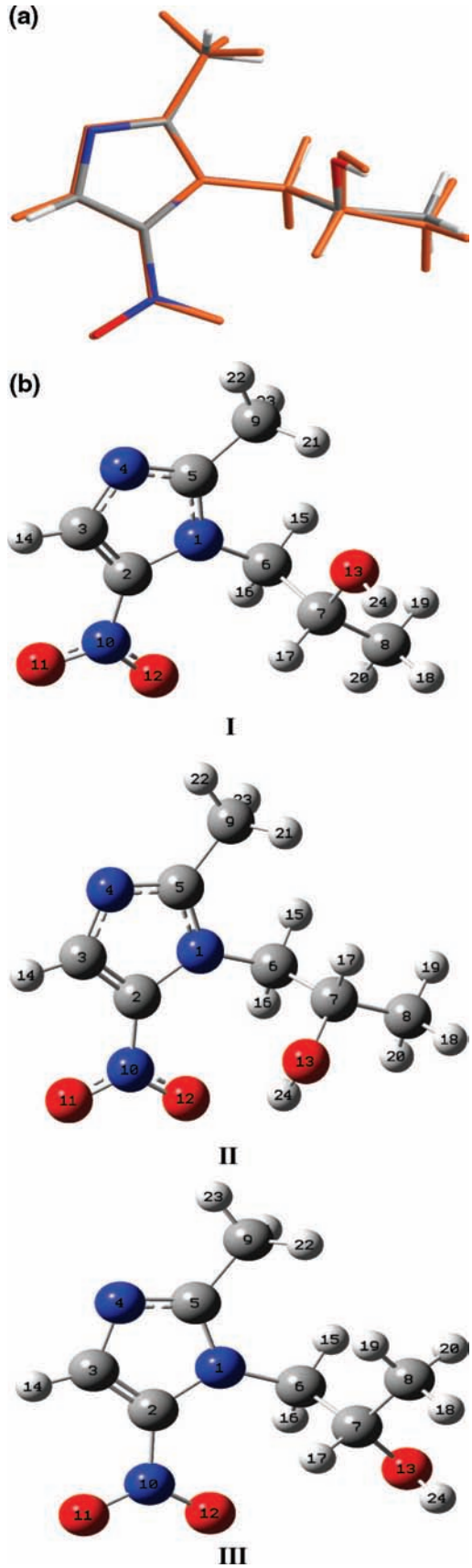

Figure 3. (a) Comparison of the experimental (from single crystal X-ray diffraction) and optimized conformations of secnidazole. (b) Equilibrium conformers of secnidazole.

no possibility of coexistence of different conformers at room temperature. The total energies are found to decrease with the increase of the basis set dimension.

The presence of negative charge on O12 atom, net positive charge on H24 atom, and small intermolecular distance (≈2 Å) between these two atoms suggests the presence of intramo-

TABLE 1: Theoretically Computed Energies (in Hartree) of Equilibrium Conformers of Secnidazole

conformer	4-31G	6-31G	6-311++G(d,p)
I	−662.281629 9	−662.970 642 9	−663.390 815 9
II	−662.280 808 8	−662.969 564 7	−663.389 408 3
III	−662.276 145 3	−662.965 239 2	−663.386 555

lecular hydrogen bonding in the crystalline phase. Using compiled data for a large number of C−H...O contacts, Desiraju et al.[19] found significant statistical directionality even as far out as 3.0 Å, and they concluded that these are to be legitimately viewed as "weak" hydrogen bonds with a greater contribution to packing forces than simple van der Waals attractions. In conformer **II**, there exists the possibility of a much stronger intramolecular hydrogen bond O13H24...O12 owing to a smaller distance of 2.106 Å between atoms H24 and O12. But in conformers **I** and **III**, the distances between atoms H24 and O12 are 4.810 and 4.316 Å, respectively, which confirm a much weaker intramolecular hydrogen bond O13H24...O12. In conformer **I**, however, there exists the possibility of another stronger intramolecular hydrogen bond C7H17...O12 owing to a smaller distance of 2.613 Å between atoms H17 and O12.

It may be seen that the DFT calculations yield comparable geometries using the same basis set for the three conformers which differ from each other by not more than 0.02 Å in bond length and 2° in bond angle except for the bond angles directly related to the moieties associated with the conformational change (the bond angle C6C7O13 increases by 6.03°, while the angle O13C7H17 decreases by 5.41° in conformer **II**).

B. Vibrational Assignments. The molecular structures of all the three equilibrium conformers of secnidazole are shown in Figure 3b. The total number of atoms in this molecule is 24; hence, it gives 66 ($3n - 6$) normal modes. The molecular conformation obtained from the crystalline structure, as well as the one yielded by geometry optimization, exhibits no special symmetries, and hence the molecule belongs to the C_1 point group. As a consequence, all the 66 fundamental vibrations of the free molecule belong to the A irreducible representation and are both IR and Raman active. As a crystalline solid, secnidazole and water molecules are placed in general sites (4*e* in the Wickoff notation) of the centrosymmetric space group $P2_1/c$ (C_{2h}^5). Considering that every crystalline structure has four molecules of secnidazole and four water molecule per unit cell (H_2O sites are half-occupied), this gives $3N - 3 = 321$, [$N = 4 \times 27 = 108$] vibrational modes (rotations of the free molecule become librational phonons; translations become acoustic phonons, which have zero frequency at the gamma point). Using the site symmetry, in accordance with the site group analysis proposed by Rousseau et al.,[20] the vibrational modes of secnidazole hemihydrate are distributed in the irreducible representations of the C_{2h} point group as follows

$$\Gamma_{\text{vib}}(309) = 78A_g + 78B_g + 77A_u + 76B_u \qquad (1)$$

and the remaining 12 modes are librational modes of the water molecule. According to the mutual exclusion principle, in the case of a centrosymmetric structure, Raman active representations are not infrared active, and vice versa. Thus, 156 and 153 vibrational modes exhibit Raman (A_g and B_g) and infrared (A_u and B_u) activity, respectively. However, in an organic crystal, the crystalline field is usually not strong enough to split the internal modes of the molecule, which become accidentally degenerate. Thus, the vibrational spectrum is mainly determined by the modes of the free molecule observed at higher frequencies, together with the lattice (translational and librational) modes in the low frequency spectral region.

The Raman scattering cross sections, $\partial\sigma_j/\partial\Omega$, which are proportional to the Raman intensities, may be calculated from the Raman scattering amplitude and predicted wavenumbers for each normal modes using the relationship[21,22]

$$\frac{\partial\sigma_j}{\partial\Omega} = \left(\frac{2^4\pi^4}{45}\right)\left(\frac{(\upsilon_0 - \upsilon_j)^4}{1 - \exp\left[\frac{-hc\upsilon_j}{kT}\right]}\right)\left(\frac{h}{8\pi^2 c\upsilon_j}\right)S_j \qquad (2)$$

where S_j and υ_j are the scattering activities and the predicted frequencies (in cm^{-1}), respectively, of the j^{th} normal mode, υ_0 is the Raman exciting frequency (in cm^{-1}), and h, c, and k are universal constants.

The calculated Raman and infrared intensities were used to convolve each predicted vibrational mode with a Lorentzian line shape (fwhm = 8 cm^{-1}) to produce simulated spectra. Assignments have been made on the basis of relative intensities, line shape, and potential energy distribution. The assigned wavenumbers for the most stable conformer (conformer **I**) along with the PED for each normal mode are given in Table 2.

C. Vibrational Wavenumbers. Comparison of calculated wavenumbers at the B3LYP/6-311++G(d,p) level with experimental values (Table 2) reveals an overestimation of the wavenumber of the vibrational modes due to neglect of anharmonicity present in a real system. Inclusion of electron correlation in density functional theory to a certain extent makes the wavenumber values smaller in comparison with the Hartree−Fock wavenumber data. The vibrational wavenumbers were obtained from the DFT calculations using a dual scaling procedure for the fingerprint region (below 1800 cm^{-1}) and X−H stretching (above 1800 cm^{-1}) regions, respectively.[24,25] All the calculated vibrational wavenumbers reported in this paper are scaled values. Experimental and calculated (scaled) Raman and infrared absorbance spectra are shown in Figures 4 and 5, respectively.

1. C−OH Vibrations. In the FT-IR spectrum of secnidazole (Figure 5), the characteristic peak corresponding to the stretching mode of the OH group is identified at 3452 cm^{-1}, whereas it is calculated to be 3667 cm^{-1}. In the Raman spectra, this band is present as a broad and weak band around 3460 cm^{-1}. In conformer **II**, this mode is calculated to be 3584 cm^{-1} with smaller intensity in comparison to the corresponding intensities in conformers **I** and **III**. The smaller value of OH stretching wavenumber can be attributed to intrachain hydrogen bonding (O13H24...O12) in conformer **II**. OH deformation modes are calculated to be 1279 and 1210 cm^{-1}, and they are observed at 1271 and 1196 cm^{-1} in the IR spectra and at 1272 cm^{-1} in the Raman spectra.

The stretching modes υ(CO) at the calculated wavenumbers 1124 and 932 cm^{-1} correspond to the observed bands at 1138 and 935 cm^{-1} in the IR spectra and at 1138 and 937 cm^{-1} in the Raman spectra. These two modes have nearly 20% contribution from υ(CO), although the contribution from $\rho(CH_3)$ is nearly 30%. This is because of heavy mixing of the modes. The vibrational modes calculated to be 486 and 468 cm^{-1} have a major contribution from the internal coordinate corresponding to the deformation of CCO. These modes are observed at 495 and 476 cm^{-1} in the Raman spectra and approximately at the

TABLE 2: Theoretical and Experimental Vibrational Wavenumbers (cm^{-1}) of Conformers of Secnidazole[a]

DFT				
unscaled	scaled	Raman	IR	PED[b]
3842	3667	—	3452	OH[υ(OH)](100)
3262	3114	3137	3133	R[υ(C3H)](99)
3158	3014	3015	3015	CH2[$\upsilon_a(CH_2)$](99)
3145	3002	3003	2998	Me1[$\upsilon_a(CH_3)$](97)
3101	2960	2984	2984	Me2[$\upsilon_a(CH_3)$](96)
3097	2956	2975	2974	Me1[$\upsilon_a(CH_3)$](74) + Me2[$\upsilon_a(CH_3)$](15) + CH2[$\upsilon(CH_2)$](7)
3096	2955	2934	2937	Me2[$\upsilon_a(CH_3)$](71) + Me1[$\upsilon_a(CH_3)$](22)
3090	2949	—	2918	CH2[$\upsilon_s(CH_2)$](83) + Me2[$\upsilon_a(CH_3)$](14)
3037	2899	2906	2896	CH[υ(C7H)](94)
3032	2894	2878	2871	Me1[$\upsilon_s(CH_3)$](99)
3028	2890	2849	2850	Me2[$\upsilon_s(CH_3)$](100)
1562	1538	1536	1529	NO2[υ_a(NO) + δ(N10C2) + $\delta(NO_2)$](63)+ R[υ(CC) + υ(NC)](26)
1540	1516	—	—	R[υ_a(NC) + δ(C3H)](34) + NO2[υ_a(NO)](22) + Me1[δ_a(CH3) + υ(CC)](14)
1504	1481	1489	1489	R[υ(NC) + δ_{ring} + υ(CC)](36) + Me1[υ(CC) + δ_a(CH3)](27) + CH2[$\delta(CH_2)$](8) + Me2[δ(CH3)](6)
1499	1476	1489	1488	R[υ(CC) + δ_{ring}](36) + NO2[υ_a(NO)](24) + Me1[$\delta_a(CH_3)$(16)]
1496	1474	—	—	Me2[$\delta_a(CH_3)$ + $\rho(CH_3)$](80)
1493	1470	—	—	Me2[$\delta_a(CH_3)$ + $\rho(CH_3)$](81) + Me1[$\delta(CH_3)$](5)
1484	1462	1471	1468	Me1[$\delta_a(CH_3)$ + $\delta(CH_3)$](89)
1472	1450	1461	1448	CH2[$\delta(CH_2)$](54) + Me1[$\delta_a(CH_3)$](21)
1454	1432	1437	1430	R[υ(NC)](32) + CH2[$\delta(CH_2)$ + υ(NC)](25) + Me1[$\delta_a(CH_3)$(15) + NO2[δ(N10C2) + υ(CN) + υ(NO)](12)
1421	1400	1408	—	CH2[$\omega(CH_2)$ + $\delta(CH_2)$](34) + CH[ρ(CH) + υ(CC)](32) + Me2[$\delta_s(CH_3)$](19) + OH[δ(OH)](7)
1415	1395	1390	1392	Me1[$\delta_s(CH_3)$(49)] + CH2[$\gamma(CH_2)$](6) + CH[ρ(CH)](5) + Me2[$\delta_s(CH_3)$](5) + R[υ_a(CN)](5) + NO2[υ(C2N10)](5)
1411	1390	—	—	Me2[$\delta_s(CH_3)$](70) + υ(CC)(9) + CH[ρ(CH)](5)
1391	1371	—	1379	NO2[υ(C2N10) + υ_a(NO) + $\delta(NO_2)$](25) + CH[ρ(CH)](20) + R[υ(CN) + δ(C3H)](25) + CH2[$\gamma(CH_2)$](15)
1387	1367	1369	1357	NO2[υ(NO) + υ(C2N10) + $\delta(NO_2)$](31) + Me1[$\delta_s(CH_3)$ (29)] + CH[ρ(CH)](16) + CH2[$\omega(CH_2)$](7) + R[υ(CN)(5)]
1379	1360	1345	1333	R[υ(NC)](36) + CH2[$\gamma(CH_2)$](22) + CH[ρ(CH)](11)
1350	1331	1307	1305	CH[ρ(CH)](49) + CH2[$\omega(CH_2)$](32)
1297	1279	1272	1271	R[υ(NC) + δ_{ring}](28) + CH2[$\gamma(CH_2)$](21) + OH[δ(OH)](20) + CH[ρ(CH)](7)
1292	1275	1265	1264	R[υ(CN) + δ(C3H) + δ_{ring} + υ(NC)](53) + NO2[υ(NC) + υ_a (NO) + δ(NO2)](37)
1226	1210	—	1196	CH2[$\rho(CH_2)$](21) + OH[δ(OH)](20) + R[υ(NC) + δ(C3H) + δ_{ring}](20) + CH[ρ(CH)](17)
1216	1201	1192	1184	R[υ(CN) + υ(CC) + δ_{ring} + υ(NC) + δ(C3H)](55) + CH2[υ(NC)](19) + NO2[υ(NO)](11) + Me1[υ(CC)](5)
1176	1164	1155	1151	R[δ_{ring} + δ(C3H) + υ_a(CN)](68) + NO2[υ(C2N10)](9) + CH2[υ(NC)](5)
1136	1124	1138	1138	Me2[$\rho(CH_3)$](30) + OH[υ(CO)](22) + δ(C8OC7)(14) + υ(CC)(7) + CH2[$\rho(CH_2)$](8)
1117	1105	1111	1110	υ(CC)(28) + Me2[$\rho(CH_3)$](25) + OH[υ_a(CO) + δ(OH)](19) + δ(CCO)(11) + CH2[δ(NC7C6)](6)
1074	1063	1086	1085	υ(CC)(32) + OH[δ(OH) + υ_a(CO)](24) + CH2[$\rho(CH_2)$](12) + δ(CCO)(6) + Me2[$\rho(CH_3)$](5)
1065	1054	1044	1039	Me1[$\rho(CH_3)$ + $\delta_a(CH_3)$ + δ_{oop}(C9C5)](85) + R[τ_{ring}](5)
1018	1008	1007	1008	Me1[$\rho(CH_3)$](46) + R[υ(NC)](20)
983	975	983	981	R[δ_{ring} + υ(NC) + δ(C3H)](50) + Me1[$\rho(CH_3)$ + υ(CC)](20) + CH2[$\rho(CH_2)$ + δ(C6N1)](7)
940	932	937	935	Me2[$\rho(CH_3)$](37) + υ(CC)(30) + OH[υ_a (CO)](20)
902	896	906	904	CH2[$\rho(CH_2)$](40) + Me2[$\delta(CH_3)$](14) + υ(CC)(9) + R[υ(NC)](11)
890	884	879	878	R[δ_{oop}(C3H) + τ_{ring}](94)
849	844	842	842	OH[υ(CO)](31) + υ(CC)(27) + Me2[$\rho(CH_3)$](12) + CH2[δ(NC7C6) +ρ(CH2)](12) + CH[ρ(CH)](5)
840	835	829	827	NO2[$\delta(NO_2)$ + υ(NC) + $\upsilon(NO_2)$](71) + R[δ_{ring}](15)
783	780	775	777	CH2[υ(NC) + δ(NC7C6)](35) + R[δ_{ring} + υ(NC)](19) + Me1[υ(CC)](13) + δ(C6C8C7)(5)
736	733	743	742	NO2[$\delta_{oop}(NO_2)$ + δ_{oop}(N10C2)](92) + R[τ_{ring}](6)
697	695	691	691	R[τ_{ring} + δ_{ring}](50) + Me1[δ_{oop}(C9C5) + υ (CC)](26)
681	681	675	675	R[τ_{ring} + δ_{ring}](57) + Me1[δ_{oop}(C9C5) + υ(CC)](24)
607	609	609	609	R[τ_{ring}](70) + NO2[δ_{oop}(N10C2)](14) + CH2[δ_{oop}(C6N1)](8)
574	576	572	569	NO2[$\rho(NO_2)$ + δ(N10C2)](52) + CH2[δ(C6N1)](12) + Me1[δ(C5C9)](12) + R[υ(CC)](5)
481	486	495	495	δ(CCO)(25) + CH2[δ(NC7C6)](11) + Me1[δ(C5C9)](10) + NO2[υ(C2N10)](7) + υ(CC)(6) + R[τ_{ring}](5)
463	468	476	475	δ(CCO)(59) + CH2[τ(N1C6) + $\rho(CH_2)$](19) + δ(C6C8C7)(8)
423	429	428	432	NO2[υ(C2N10) + δ(NO2) + ρ(NO2)](31) + δ(CCO)(24) + R[δ_{ring}](10) + CH2[δ(C6N1)](9)
391	398	395	—	NO2[δ(OC2N10) + υ(C2N10)](28) + Me1[δ(C5C9)](24) + CH2[δ(C6N1)](16) + R[υ(N1C2)](8)
336	344	351	—	CH2[δ(C6N1) + $\delta(CH_2)$ + δ_{oop}(C6N1)](32) + Me1[δ(C5C9)](22) + δ(C6C8C7)(18)
309	318	331	—	CH2[δ(C6N1) + υ(N1C6)](16) + δ(C6C8C7)(15) + δ(CCO)(12) + Me1[δ_{oop}(C9C5)](12) + NO2[$\rho(NO_2)$](10)
284	284	298	—	Me1[δ_{oop}(C9C5)](32) + NO2[δ_{oop}(N10C2)](28) + CH2[τ(N1C6)](8) + R[τ_{ring}](7)
260	271	278	—	CH2[δ_{oop}(C6N1) + δ(C6N1) + δ(NC7C6)](30) + NO2[δ_{oop}(N10C2)](20) + δ(C6C8C7)(18) + δ(CCO)(13) + Me1[δ(C5C9)](5)
232	243	—	—	OH[τ(CO)](83)
226	237	234	—	Me2[τ(C7C8)](59) + NO2[δ(N10C2)](15) + OH [τ(CO)](10) + Me1[δ(C5C9)](5)
211	223	221	—	NO2[δ(N10C2) + $\rho(NO_2)$](43) + Me2[τ(C7C8)](33) + Me1[δ(C5C9)](6) + δ(C6C8C7)(5)
147	161	169	—	Me1[τ(C5C9)](86)
136	150	147	—	NO2[δ_{oop}(N10C2)](41) + CH2[δ(NC7C6) + δ_{oop}(C6N1) + τ(N1C6)](30) + Me1[δ_{oop}(C9C5)](8) + R[τ_{ring}](5)
101	117	123	—	CH2[τ(N1C6) + δ_{oop}(C6N1) + δ(NC7C6)](42) + NO2[τ(C2N10)](39)
77	93	92	—	CH2[τ(N1C6) + δ_{oop}(C6N1) + δ(NC7C6)](77) + NO2[δ_{oop}(N10C2)](8)
60	76	75	—	(C6C7)(55) + NO2[τ(C2N10)](14) + CH2[τ(N1C6) + δ(C6N1)](14)
43	60	60	—	CH2[τ(N1C6) + δ_{oop}(C6N1)](47) + NO2[τ(C2N10) + δ_{oop}(N10C2)](31) + τ(C6C7)(9)
—	—	43	—	lattice

[a] Proposed assignment and potential energy distribution (PED) for vibrational normal modes. Types of vibration: υ, stretching; δ, deformation; oop, out-of-plane bending; ω, wagging; γ, twisting; ρ, rocking; τ, torsion. The imidazole ring modes are labeled following Wilson's notation.[23] [b] Potential energy distribution (contributing ≥5) for conformer **I**.

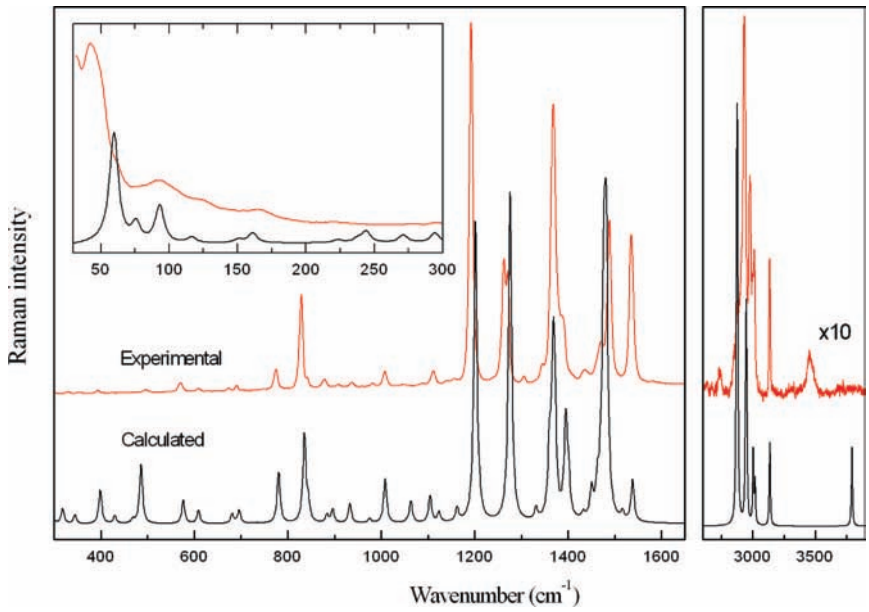

Figure 4. Experimental and calculated (scaled) Raman spectra of the secnidazole in the regions 300−1650 and 2600−3900 cm^{-1}. (Inset shows Raman spectra in the region 30−300 cm^{-1}.)

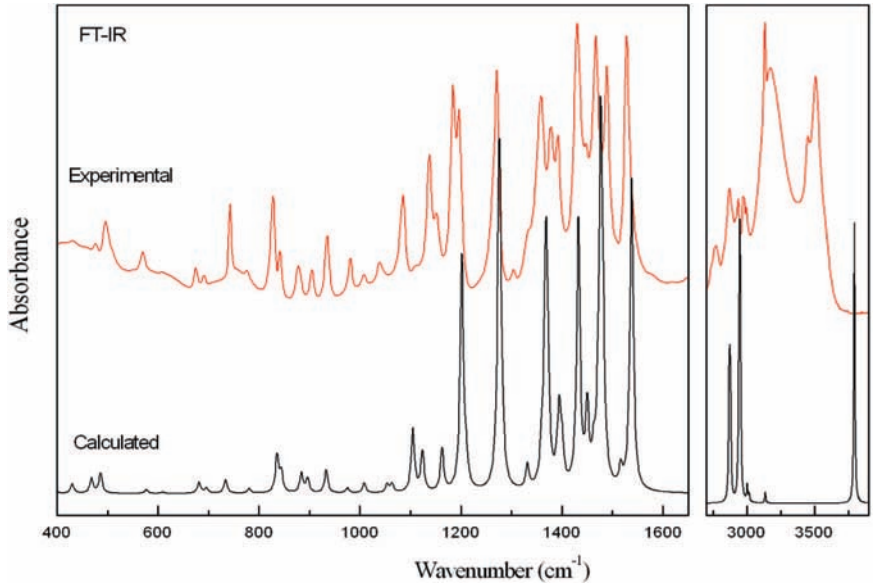

Figure 5. Experimental and calculated (scaled) infrared absorbance spectra of the secnidazole in the regions 400−1650 and 2700−3900 cm^{-1}.

same positions in the IR spectra also. The torsion around CO is calculated to be 243 cm^{-1}.

2. CC and CH Vibrations. CC stretches are calculated to be 1105, 1063, and 844 cm^{-1}, and the corresponding bands are observed at 1111, 1086, and 842 cm^{-1} in both the IR and Raman spectra. The C7−H stretch predicted at 2899 cm^{-1} by DFT calculation is in an excellent agreement with the experimental recorded bands at 2906 cm^{-1} in the Raman spectra and 2896 cm^{-1} in the IR spectra. The CH rocking mode is calculated to be 1331 cm^{-1}. The corresponding band is observed at 1305 cm^{-1} in the IR spectra and at 1307 cm^{-1} in the Raman spectra.

3. N−CH_2 Group Vibrations. The molecule contains a CH_2 group connected to the ring. The asymmetric CH_2 stretching vibration is calculated to be 3014 cm^{-1} and matches well with the IR and Raman wavenumbers. The symmetric CH_2 stretching mode is calculated to be 2949 cm^{-1}, and it is assigned to the 2918 cm^{-1} band in the IR spectra. The CH_2 deformation mode is calculated to be 1450 cm^{-1}, and the corresponding peak is observed at 1461 cm^{-1} in the Raman spectra and at 1448 cm^{-1} in the IR spectra. The CH_2 wagging mode occurs at 1305 cm^{-1} in the IR spectra and at 1408 and 1307 cm^{-1} in the Raman spectra. The calculated values are 1400 and 1331 cm^{-1}. The rocking modes of the CH_2 group give rise to the medium intensity bands at 1196 and 904 cm^{-1} in the IR spectra, and only one Raman band at 906 cm^{-1} is observed. The corresponding calculated wavenumbers are 1210 and 896 cm^{-1}, as shown in Table 2.

4. C−CH_3 Group Vibrations. Two methyl groups are present in the molecule. One of them is directly connected to the ring, and the other one is connected to the CH group. The CH_3 group has several modes associated with it, such as symmetric and asymmetric stretches, bends, and rock and torsional modes. Assignments of all these fundamentals are given in Table 2. In the first methyl group $\upsilon_s(CH_3)$ mode is observed at 2878 cm^{-1} and $\upsilon_a(CH_3)$ modes are observed at 3003 and 2975 cm^{-1} in the Raman spectra. A $\upsilon_s(CH_3)$ stretching mode is calculated to be 2894 cm^{-1}, and two $\upsilon_a(CH_3)$ asymmetric stretching modes are calculated to be 3002 and 2956 cm^{-1}. In

the IR spectra, $\upsilon_a(CH_3)$ modes are observed at 2998 and 2974 cm^{-1} and a $\upsilon_s(CH_3)$ mode is observed at 2871 cm^{-1}. The peak corresponding to symmetric stretching mode is relatively strong. We have observed the asymmetric deformation modes Me1[$\delta_a(CH_3)$] at 1468 and 1448 cm^{-1} in the IR spectra and at 1471 and 1461 cm^{-1} in the Raman spectra. These modes are calculated to be 1462 and 1450 cm^{-1}. The symmetric Me1[$\delta_s(CH_3)$] modes are assigned to the observed peaks at 1390 and 1369 cm^{-1} in the Raman spectra and at 1392 and 1357 cm^{-1} in the IR spectra. The corresponding calculated values are 1395 and 1367 cm^{-1}. The CH_3 rocking modes are assigned to weak Raman peaks at 1044 and 1007 cm^{-1} and the IR peaks at 1039 and 1008 cm^{-1} for the first methyl group. The calculated values of CH_3 rocking mode are obtained at 1054 and 1008 cm^{-1}. The calculated wavenumber at 161 cm^{-1} shows a major contribution from CH_3 torsion around the C5−C9 bond, and this matches well with the observed wavenumber (169 cm^{-1}) in the Raman spectra. A comparatively low value of this mode is due to the heavy imidazole ring attached with the C5−C9 bond. We have calculated the out-of-plane deformation at 284 cm^{-1}, and it is observed at 298 cm^{-1} in the Raman spectra. The asymmetric stretch mode of second methyl group is calculated to be 2955 cm^{-1} and matches well with the peak observed at 2934 cm^{-1} in the Raman spectra and approximately at the same position in the IR spectra. The symmetric stretch of methyl group is calculated to be 2890 cm^{-1} and matches well with 2849 cm^{-1} observed in both Raman and IR spectra. The symmetric methyl deformation mode Me2[$\delta_s(CH_3)$] is calculated to be 1390 cm^{-1} and the asymmetrical Me2[$\delta_a(CH_3)$] are calculated to be 1474 and 1470 cm^{-1}, their intensities being less than the corresponding intensities in the two other conformers. The CH_3 modes calculated for conformer **I** are in better agreement with the observed spectra in comparison to that for the other two conformers. This may be due to the different orientations of the CH_3 group in these two conformers in comparison to single crystal data. The CH_3 rocking mode is assigned to weak Raman peaks at 1138 and 1111 cm^{-1} and strong IR peaks at 1138 and 1110 cm^{-1}. These two rocking modes are calculated to be 1124 and 1105 cm^{-1}. The torsional mode C7−C8 for the second methyl group is calculated to be 237 cm^{-1}, and it matches well with the observed band in the Raman spectra.

5. C−NO_2 Vibrations. The molecule under investigation possesses only one NO_2 group, and hence one expects a symmetric and an asymmetric N−O stretching vibration of the NO_2 group. The symmetric and asymmetric stretching modes appear at 1367 and 1538 cm^{-1}, respectively, and both the modes are highly mixed modes. Symmetrical and asymmetrical deformations of the NO_2 group appear at 827/829 cm^{-1} and 742/743 cm^{-1} in IR/Raman spectra. These modes are calculated to be 835/733 cm^{-1}, respectively. The rocking mode of the NO_2 group is observed at 572 cm^{-1} in the Raman spectra. It is calculated to be 576 cm^{-1} and is assigned to the peak at 569 cm^{-1} in the IR spectra. It is also a mixed mode containing the contribution from C−N deformation. The stretching mode of C−N band (connecting NO_2 group and ring) is calculated to be 1371 cm^{-1} and has been assigned to the 1379 cm^{-1} band in the IR spectra. The C−N deformation is calculated to be 223 cm^{-1}. The C−N out-of-plane deformation is calculated to be 150 cm^{-1}, and it is assigned to a band at 147 cm^{-1} in the Raman spectra. The mode with the lowest wavenumber is the torsion mode of C−N. C−N torsions are calculated to be 117 and 60 cm^{-1}, and they are observed at 123 and 60 cm^{-1} in the Raman spectra.

6. Ring Vibrations. The C−H stretching vibration in ring is usually strong in both the IR and Raman spectra. The υ(CH) wavenumber in ring is assigned at 3137 cm^{-1} in the Raman spectra and at 3133 cm^{-1} in the IR spectra. It is calculated to be 3114 cm^{-1}, and thus coincides well with the experimental observations. The calculated wavenumber at 1516 cm^{-1} has major contribution from CN asymmetric stretching in the imidazole ring. The major contribution of the symmetric stretching mode of CN in imidazole ring is obtained in the vibrational modes at 1432 and 1360 cm^{-1}, and these are observed at 1430 and 1333 cm^{-1} in the IR spectra and at 1437 and 1345 cm^{-1} in the Raman spectra. The symmetric stretching mode R[υ(CN)] is calculated to be 1275 and 1201 cm^{-1} mixed with R[υ(CC)] symmetric stretch and other modes. It corresponds to the peaks at 1265 and 1192 cm^{-1} in the Raman spectra and at 1264 and 1184 cm^{-1} in the IR spectra. R[υ(CC)] symmetric stretches are calculated to be 1538 and 1476 cm^{-1} and are assigned to the bands at 1529 and 1488 cm^{-1} in the IR spectra and at 1536 and 1489 cm^{-1} in the Raman spectra.

Ring deformations are calculated to be 1164 and 975 cm^{-1}, and these are observed at 1155 and 983 cm^{-1} in the Raman spectra and at 1151 and 981 cm^{-1} in the IR spectra. Out-of-plane deformation of R[δ_{oop}(C3H)] is calculated to be 884 cm^{-1} and matches well with IR and Raman spectra. The torsions of the ring are calculated to be 695, 681, and 609 cm^{-1}. These are also in excellent agreement with the experimentally observed IR and Raman values.

By using a subtractive triple spectrometer, the low energy region of the Raman spectrum is easily recorded (inset of Figure 4).[26] This equipment provides an excellent rejection of the excitation line lowering the spectral limit down to 30 cm^{-1} when compared with single and Fourier transform spectrometers. The extended spectral range allows us to observe the lattice and skeleton vibrational modes, which are expected to be directly related to the crystal structure. Our results show an excellent agreement between the calculated and experimental values in this spectral region, allowing us to establish a detailed assignment of all these bands. Just one band, located at 43 cm^{-1}, could not be associated with any vibrational mode of the single molecule, and this has been classified as a lattice vibration. It is interesting to notice that usually the lattice vibrations are observed below 200 cm^{-1}. However, our results show that these types of modes are in the very low wavenumber region, probably below 50 cm^{-1}. All the modes above 50 cm^{-1} were classified as deformations and torsions of the secnidazole molecule. On the other hand, the lattice modes associated with the translations and librations of the whole molecule lie below 50 cm^{-1} and can only be observed by dispersive Raman (in a subtractive spectrometer), far-infrared, or terahertz spectroscopy.

By comparing the rest of the vibrational spectra of secnidazole with the help of the PED distribution presented in Table 2, we find a very good overall agreement. The difference between the observed and scaled wavenumber values of most of the fundamentals is quite small.

Finally, in Figure 6, a selected spectral region of the calculated Raman spectrum is compared with experimental data obtained at 30 and 90 °C. The room temperature Raman spectrum corresponds to the hemihydrate form discussed previously. On the other hand, secnidazole is in the melted form at 90 °C since its melting point is 70 °C.[2] As stated previously, our DFT results reproduce very well the experimental data, but interesting features may be identified between the two experimental spectra recorded at 30 and 90 °C. First, we notice that the band at 1192 cm^{-1} remains approximately unaltered in the melted state. This

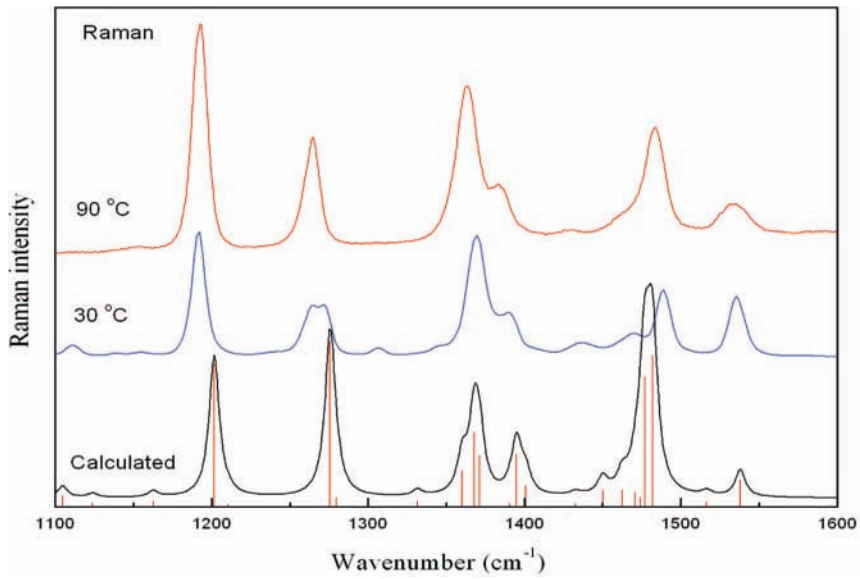

Figure 6. Comparison of the Raman spectra of the secnidazole in the hemihydrate (30 °C) and melted (90 °C) forms with the one obtained from DFT calculations (scaled).

band is associated with the breathing of the imidazole ring. In the solid form, this ring participates in the hydrogen bond pattern that stabilizes the crystalline structure through a OH···N bond. However, this interaction does not seem to be strong enough to affect the ring breathing frequency. The neighboring bands, located at 1265 and 1272 cm^{-1}, exhibit a different behavior. At room temperature they split into two bands (1265 and 1272 cm^{-1}) and merge into just one band (1265 cm^{-1}) at 90 °C. According to Table 2, the first one at 1265 cm^{-1} is related to the deformation of the imidazole ring of the nitro group, whereas the second one at 1272 cm^{-1} has contributions from the deformations of the ring as well as methylene and hydroxyl groups. Even though DFT calculations have predicted a negligible Raman intensity for the latter, this is one of the most intense bands in the Raman spectrum. This anomalous behavior could be explained by considering that the hydroxyl group participates in all the main intermolecular interactions in the solid hemihydrate form. The change in the vibrational mode polarizability due to these interactions may easily affect its Raman cross section. Nevertheless, the loss of the intermolecular hydrogen bonds in the melted form reduces the intensity of this band since the molecule now acquires a configuration which is closer to single molecule approximation that is taken in the theoretical model. The remaining bands observed in the spectral region presented in Figure 6 do not present any evidence of other effects that produce shift and line broadening, which are expected in a completely disordered liquid.

V. Conclusions

Geometry optimizations show that there are three conformers of secnidazole having very close total energies. Thus, calculations using DFT at the B3LYP level with extended basis sets 4-31G, 6-31G, and 6-311++G(d,p), show that the energy differences between the reported conformers are as small as 0.5−3.0 kcal mol^{-1}. However, these energy differences are much larger than *kT*, so there is almost no possibility of coexistence of different conformers at room temperature. X-ray diffraction study also confirms that just one of them (conformer **I**) was identified in the crystalline structure of secnidazole hemihydrate. The optimized structure of this conformer is very close to the one observed experimentally (bond lengths differ by less than 0.01 Å and bond angles differ by about 1°, except for the moieties where the difference is almost 6°). In conformer **I**, there exists the possibility of stronger intramolecular hydrogen bond C7H17...O12 owing to a smaller distance of 2.613 Å between atoms H17 and O12. Vibrational spectroscopy and DFT calculations have been applied for investigating the most stable conformer of secnidazole. Raman and infrared spectra were recorded, and the vibrational bands were assigned on the basis of the PED obtained from the DFT calculations. In general, a very good agreement between experimental and calculated modes was observed. A striking feature of the work is that the study of vibrational spectra and DFT calculations reveals that the lattice modes of secnidazole lie below 50 cm^{-1}. However, such low-lying modes can only be observed by using high performance spectroscopic techniques.

Acknowledgment. The financial support to one of the authors (P.T.) from the Alexanded von Humboldt Foundation, Germany, is gratefully acknowledged. A.P.A. and S.B.H. acknowledge the financial support of the Brazilian agencies CNPq, CAPES and FUNCAP. Authors would like to thank Vineet Gupta for computational support.

References and Notes

(1) *Martindale the Extra Pharmacopoeia*, 27 ed.; The Pharmaceutical Press: London, 1977; p 1570.

(2) Boza, A.; Gonzalez, R.; Novoa, H.; Cuéllar, D. M.; Valdés, M. *IL Farmaco* **2000**, *55*, 700.

(3) Gillis, J. C.; Wiseman, L. R. Secnidazole: a review of its antimicrobial activity, pharmacokinetic properties and therapeutic use in the management of protozoal infections and bacterial vaginosis. *Drugs* **1996**, *51*, 621.

(4) Soedin, K.; Syukran, O.; Fadillah, A.; Sidabutar, P. *Pharmaceutica* **1985**, *4*, 251.

(5) Novoa, H.; González, R.; Dago, A.; Pomés, R.; Li, N. Estructura cristalina del (hidroxi-2-propil)-1-metil-2-nitro-5-imidazol hemi-hidratado. *Rev. CENIC Ciencias Quim.* **1997**, *28*, 89.

(6) *Handbook of Vibrational Spectroscopy*; Chalmers, J. M., Griffiths, P. R., Eds.; John Wiley & Sons: New York, 2002.

(7) Rodríguez-Carvajal, J. FULLPROF: A Program for Rietveld Refinement and Pattern Matching Analysis; Satellite Meeting on Powder Diffraction of the XV IUCr Congress, 1990; p 127.

(8) Hohenberg, P.; Kohn, W. *Phys. Rev. B* **1964**, *864*, 136.

(9) Frisch, M. J.; Trucks, G. W.; Schlegel, H. B.; Scuseria, G. E.; Robb, M. A.; Cheeseman, J. R.; Montgomery, J. A.; Vreven, T.; Kudin, K. N.;

Burant, J. C.; Millam, J. M.; Iyengar, S. S.; Tomasi, J.; Barone,V.; Mennucci, B.; Cossi, M.; Scalmani, G.; Rega, N.; Petersson, G. A.; Nakatsuji, H.; Hada, M.; Ehara,M.; Toyota, K.; Fukuda, R.; Hasegawa, J.; Ishida, M.; Nakajima; Honda, Y.; Kitao, O.; Nakai, H.; Klene, M.; Li, X.; Knox, J. E.; Hratchian, H. P.; Cross, J. B.; Adamo, C.; Jaramillo, J.; Gomperts, R.; Stratmann, R. E.; Yazyev, O.; Austin, A. J.; Cammi, R.; Pomelli, C.; Ochterski, J. W.; Ayala, P. Y.; Morokuma, K.; Voth, G. A.; Salvadorm, P.; Dannenberg, J. J.; Zakrzewski, V. G.; Dapprich, S.; Daniels, A. D.; Strain, M. C.; Farkas, O.; Malick, D. K.; Rabuck, A. D.; Raghavachari, K.; Foresman, J. B.; Ortiz, J. V.; Cui, Q.; Baboul, A. G.; Clifford, S.; Cioslowski, J.; Stefanov, B. B.; Liu, G.; Liashenko, A.; Piskorz, P.; Komaromi, I.; Martin, R. L.; Fox, D. J.; Keith, T.; Al-Laham, M. A.; Peng, C. Y.; Nanayakkara, A.; Challacombe, M.; Gill, P. M. W.; Johnson, B.; Chen, W.; Wong, M. W.; Gonzalez, C.; Pople, J. A. Gaussian 03, Revision C.02; Gaussian, Inc., Wallingford, CT 06492, 2003.

(10) Lee, C. T.; Yang, W. T.; Parr, R. G. *Phys. Rev. B* **1988**, *37*, 785.

(11) Parr, R. G.; Yang, W. *Density Functional Theory of Atoms and Molecules*; Oxford University Press: New York, 1989.

(12) Becke, A. D. *J. Chem. Phys.* **1993**, *98*, 5648.

(13) Petersson, G. A.; Allaham, M. A. *J. Chem. Phys.* **1991**, *94*, 6081.

(14) Petersson, G. A.; Bennett, A.; Tensfeldt, T. G.; Allaham, M. A.; Shirley, W. A.; Mantzaris, J. *J. Chem. Phys.* **1988**, *89*, 2193.

(15) Pulay, P.; Fogarasi, G.; Pang, F.; Boggs, J. E. *J. Am. Chem.Soc.* **1979**, *101*, 2550.

(16) Fogarasi, G.; Zhou, X.; Taylor, P. W.; Pulay, P. *J. Am. Chem.Soc.* **1992**, *114*, 8191.

(17) Martin, J. M. L.; Van Alsenoy, C. Gar2ped; University of Antwerp; 1995.

(18) Zhurko, G. A.; Zhurko, D. A. Chemcraft Available from http://www.chemcraftprog.com, **2005**.

(19) Desiraju, G. R.; Steiner, T. *The Weak Hydrogen Bond*; Oxford University Press: New York, 1999; p13.

(20) Rousseau, D. L.; Bauman, R. P.; Porto, S. P. S. *J. Raman Spectrosc.* **1981**, *10*, 253.

(21) Guirgis, G. A.; Klaboe, P.; Shen, S.; Powell, D. L.; Gruodis, A.; Aleksa, V.; Nielsen, C. J.; Tao, J.; Zheng, C.; Durig, J. R. *J. Raman Spectrosc.* **2003**, *34*, 322.

(22) Polavarapu, P. L. *J. Phys. Chem.* **1990**, *94*, 8106.

(23) Varsanyi, G. *Vibrational Spectra of Benzene Derivatives*; Academic Press: New York, 1969.

(24) Halls, M. D.; Velkovski, J.; Schlegel, H. B. *Theor. Chem. Acc.* **2001**, *105*, 413.

(25) Ayala, A. P.; Siesler, H. W.; Wardell, S. M. S.; Boechat, V. N.; Dabbene, V.; Cuffini, S. L. *J. Mol. Struct.* **2007**, *828*, 201.

(26) Ayala, A. P. *Vib. Spectrosc.* **2007**, *45*, 112.

JP805399H